The catalytic removal of CO and NO over Co–Pt(Pd, Rh)/γ-Al_2O_3 catalysts and their structural characterizations

Ming Meng, Pei-yan Lin* and Yi-lu Fu

Department of Chemical Physics, University of Science and Technology of China, Hefei 230026, PR China

Received 7 May 1997; accepted 12 September 1997

A series of Co–Pt(Pd, Rh)/γ-Al_2O_3 catalysts were prepared by successive wetness impregnation. The catalytic activities for CO oxidation, NO decomposition and NO selective catalytic reduction (SCR) by C_2H_4 over the samples calcined at 500°C and reduced at 450°C were determined. The activities of the samples calcined at 750°C and reduced at 450°C for NO selective catalytic reduction (SCR) by C_2H_4 were also determined. All the samples were characterized by XRD, XPS, XANES, EXAFS, TPR, TPO and TPD techniques. The results of activity measurements show that the presence of noble metals greatly enhances the activity of Co/γ-Al_2O_3 for CO or C_2H_4 oxidation. For NO decomposition, the H_2-reduced Co–Pt(Pd, Rh)/γ-Al_2O_3 catalysts exhibit very high activities during the initial period of catalytic reaction, but with the increase of reaction time, the activities decrease obviously because of the oxidation of surface cobalt phase. For NO selective reduction by C_2H_4, the reduced samples are oxidized more quickly by the excess oxygen in reaction gas. The oxidized samples possess very low activities for NO selective reduction. The results of XRD, XPS and EXAFS indicate that all the cobalt in Co–Pt(Pd, Rh)/γ-Al_2O_3 has been reduced to zero valence during reduction by H_2 at 450°C, but in Co/γ-Al_2O_3 only a part of the cobalt has been reduced to zero valence, the rest exists as $CoAl_2O_4$-like spinel which is difficult to reduce. For the samples calcined at 750°C, the cobalt exists as $CoAl_2O_4$ which cannot be reduced by H_2 at 450°C and possesses better activities for NO selective reduction. The results of XANES spectra show that the cobalt in Co/γ-Al_2O_3 has lower coordination symmetry than that in Co–Pt(Pd, Rh)/γ-Al_2O_3. This difference mainly results from the distorting tetrahedrally-coordinated Co^{2+} ions which have lower coordination symmetry than Co^0 in the catalysts. The coordination number for the Co–Co shell from EXAFS has shown that the cobalt phase is highly dispersed on Co–Pt(Pd, Rh)/γ-Al_2O_3 catalysts. The TPR results indicate that the addition of noble metals to Co/γ-Al_2O_3 makes the TPR peaks shift to lower temperatures, which implies the spillover of hydrogen species from noble metals to cobalt oxides. The oxygen spillover from noble metals to cobalt is also inferred from the shift of TPO peaks to lower temperatures and the increased amount of desorbed oxygen from TPD. For CO oxidation, the Co^0 is the main active phase. For NO decomposition and selective reduction, Co^0 is also catalytically active, but it can be oxidized into Co_3O_4 by oxygen at high reaction temperature.

Keywords: Co–Pt(Pd, Rh)/γ-Al_2O_3 catalysts, CO oxidation, NO decomposition, NO SCR, structural characterization, synergy effect

1. Introduction

Although the three-way automotive catalysts mainly composed of noble metals have successfully controlled the exhaust emissions from conventional gasoline engines [1–4], the nitrogen oxides (NO_x) in the exhaust from lean-burn gasoline engines and diesel engines can be removed only with low conversion on such catalysts. Ammonia as a conventional reductant for NO_x selective reduction has many disadvantages, such as transportation and storage hazards, equipment erosion and NH_3 slip. While using hydrocarbons as reductants, such problems can be avoided. Some studies [5,6] have shown that some metal ion-exchanged zeolite catalysts, such as Cu-ZSM-5 and Co-ZSM-5, are active for the selective reduction of NO in the presence of excess oxygen, however, a volcano-like activity dependence on reaction temperature is observed for these kinds of zeolite catalysts because of the low structural stability of zeolites, the complete oxidation of reductants and the dealumination of zeolite framework by water vapor at high reaction temperature. Therefore, there is a need to study the non-zeolite catalysts for NO selective reduction. Some rare earth oxides [7] and some catalysts for methane oxidative coupling [8,9] have been reported to be also active for NO selective reduction by methane.

It has been reported that the cobalt-based catalysts are active for many catalytic reactions, such as Fischer–Tropsch synthesis [10], CO oxidation [11], NO reduction by some hydrocarbons [12–14] and NO decomposition [15,16]. Recently, several new cobalt-based catalysts promoted by small amounts of noble metals are reported to be very effective for car exhaust purification [17] or other catalytic reactions [18]. These studies have indicated that the presence of a small amount of noble metals has greatly enhanced the activity of the cobalt-based catalysts. Lin et al. [17] have reported that the initial activity of the alumina-supported $La_{0.45}Sr_{0.15}Ce_{0.35}Zr_{0.05}Co_{1.0}$ promoted with 0.49 mg Pt–Rh per gram catalyst can be comparable to a commercial three-way catalyst (TWC) which contains more than four times as much Pt–Rh. Schanke et al. [18] have reported that the addition of a

* To whom correspondence should be addressed.

small amount of platinum (0–0.4 wt%) to γ-Al_2O_3-supported cobalt catalysts has greatly improved the CO hydrogenation activity and the selectivity to alcohol. The study by Guczi et al. [19] has shown that the CO hydrogenation activity and the selectivity to alcohol over the cobalt-based catalysts promoted by noble metals have increased with the increasing content of noble metals. Many studies [17–20] have shown that the the presence of noble metals enhances not only the reduction deepness of oxidized samples, but also the oxidation of reduced samples. Similar results have been obtained by Sass et al. [21] over Co–Pd/γ-Al_2O_3 catalysts and by van't Blik and Prins [22] over a Co–Rh/SiO_2 system. A series of Co–Pt/Al_2O_3 catalysts with various Pt/Co ratios have been studied by Guzci and coworkers [19,23,24], and the formation of Co–Pt bimetallic particles has been confirmed by the extended X-ray absorption fine structure (EXAFS) method [25–27].

Up to now, the alumina-supported cobalt catalysts promoted with Pt, Pd or Rh have not been reported to be used both for NO selective reduction and for CO oxidation. The correlation between the activities and structures on such catalysts has not been clarified, and the effects of noble metals on Co/γ-Al_2O_3 have not been studied extensively either. In this study, the catalytic activities of Co/γ-Al_2O_3 promoted by noble metals both for CO oxidation and for NO selective catalytic reduction by C_2H_4 are evaluated. The structures of Co–Pt(Pd, Rh)/γ-Al_2O_3 catalysts are characterized by X-ray diffraction (XRD), X-ray photoelectron spectroscopy (XPS), X-ray absorption fine structure (XAFS) and temperature-programmed reduction (TPR), oxidation (TPO) and desorption (TPD). The effect of noble metals on Co/γ-Al_2O_3 is investigated from the cobalt valence, cobalt phase dispersion and spillover effect of hydrogen and oxygen from noble metals to cobalt phases.

2. Experimental

2.1. Sample preparation

The support γ-Al_2O_3 (BET area: 157 m^2/g) was obtained from $Al(OH)_3$ gel (produced by the Third Petroleum Factory of Fushun, China) which was calcined in air at 750°C for 16 h. Before use, the γ-Al_2O_3 was pelletized and sieved to 40–60 mesh.

The samples were prepared by successive wetness impregnation. A given amount of $Co(NO_3)_2{\cdot}6H_2O$ aqueous solution was first impregnated on γ-Al_2O_3. After drying at 120°C and calcination at 500°C for 2 h, the solution of $H_2PtCl_6{\cdot}6H_2O$, $PdCl_2$ or $RhCl_3{\cdot}3H_2O$ was impregnated on the precursor of Co/γ-Al_2O_3, respectively. After drying at 120°C and calcining at 500°C in air for 2 h, the samples were reduced by hydrogen at 450°C for 1 h.

For NO selective reduction by C_2H_4, the precursor of Co/γ-Al_2O_3 was also calcined at 750°C for 2 h. After the noble metals had been impregnated on it, the samples were reduced under the same conditions. The contents of cobalt and noble metals in the samples are Co_3O_4/Al_2O_3 = 8 wt% and noble metal/catalyst = 0.1 wt%, respectively.

2.2. Measurements of catalytic activities

The catalytic activities of the samples for CO oxidation and NO reduction by C_2H_4 were measured in a gas-flowing micro-reactor. The reactor is a stainless steel tube with 6 mm inner diameter. The sample used was 200 mg.

For CO oxidation, the reaction gas is composed of CO: 0.5%, O_2: 5% and N_2: 94.5%. The gas hourly space velocity (GHSV) was 4500 h^{-1}. The effluent gas from the reactor was analyzed by a gas chromatograph equipped with a 2 m column with 5A molecular sieves and a thermal conductivity detector (TCD).

For NO decomposition, the reaction gas contains 1800 ppm NO balanced with pure helium (99.99%). For NO selective reduction by C_2H_4, the reaction gas is composed of 1000 ppm C_2H_4, 1600 ppm NO and 2.5% O_2 balanced with helium. $W/F = 0.6$ g s cm^{-3}. The effluent gas from the reactor was analyzed by an on-line quadrupole mass spectrometer (LZL-203 type) and an electrochemical NO_x analyzer (BDEP-01 type). The conversion of C_2H_4 was calculated by the production of CO_2. The NO conversion was determined directly by the NO_x analyzer.

2.3. Sample characterization

2.3.1. XRD

XRD patterns were recorded on a D/MAX-rA rotatory target diffractometer using Cu Kα ($\lambda = 0.15418$ nm) as X-ray source.

2.3.2. XPS

XPS spectra were recorded on an ESCALAB MK-II spectrometer using Al Kα ($E = 1486.6$ eV) as X-ray source. The Al 2p peak (74.5 eV) from the samples was used as an internal standard for binding energy calibration.

2.3.3. XAFS

Co K-edge (7709.7 eV) XAFS spectra were recorded on the XAFS station, 4W1B beam line of Beijing Synchrotron Radiation Facility of National Laboratory (BSRF NL). The critical beam energy was 2.2 GeV with a storage ring current of ~ 50 mA. The transition mode was used to record XAFS data. A Si(111) double-crystal monochromator was used to reduce the harmonic content of the monochromator beam. Both X-ray absorption near edge structure (XANES) and extended X-ray absorption fine structure (EXAFS) were studied. The

back-subtracted EXAFS function was converted into k space and weighted by k^3 in order to compensate for the diminishing amplitude due to the decay of the photoelectron wave. The EXAFS structural parameters of samples were obtained by curve-fitting. Co metal, Co_3O_4 and $CoAl_2O_4$ were used as model compounds.

2.3.4. TPR

The H_2-TPR investigation was carried out with a mixture of H_2/N_2 (1 : 19, 30 ml/min) in a conventional flow system. Before the mixture gas passed through the sample (200 mg, 40–60 mesh) in a U-shaped stainless steel micro-reactor, it was purified by passing through deoxidizer and 5A molecular sieve. The reaction temperature was increased at a rate of 10°C/min. The effluent gas was analyzed by a gas chromatograph with TCD.

2.3.5. TPD

The O_2-TPD investigation was performed in a conventional temperature programming system equipped with a TCD for analysis. The catalyst sample (500 mg) was pretreated in helium (99.99%) at 500°C for 1 h, then the oxygen adsorption was proceeded with 8% O_2/N_2 at 200°C for 0.5 h. After cooling to room temperature in O_2/N_2 mixture, the O_2-TPD measurement was performed using helium as carrier gas. The temperature was increased at a rate of 10°C/min from room temperature to 700°C.

2.3.6. TPO

The TPO experiment was carried out in a stainless micro-reactor with 6 mm inner diameter. The reaction gas is composed of O_2/N_2 (1 : 99). The sample used is 500 mg. The temperature was elevated at a rate of 5°C/min from room temperature to 600°C. The oxygen concentration in the effluent gas was determined by an online quadrupole mass spectrometer.

3. Results and discussion

3.1. Activities for catalytic reactions

3.1.1. CO oxidation

The relationships between CO conversion and reaction temperature on various catalysts are shown in figure 1.

Figure 1 shows that the Co/γ-Al_2O_3 catalyst possesses good activity for CO oxidation. At the temperature of 200°C, the CO is completely oxidized. When a small amount of noble metals is added to Co/γ-Al_2O_3, the activity for CO oxidation is greatly enhanced. Compared with Co/γ-Al_2O_3, the reaction temperature for CO 100% conversion decreased by about 60°C over Co–Pt(Pd)/γ-Al_2O_3 catalysts. For Co–Rh/γ-Al_2O_3, the corresponding temperature decreased by 25°C approximately, but at the region of low temperature (< 150°C),

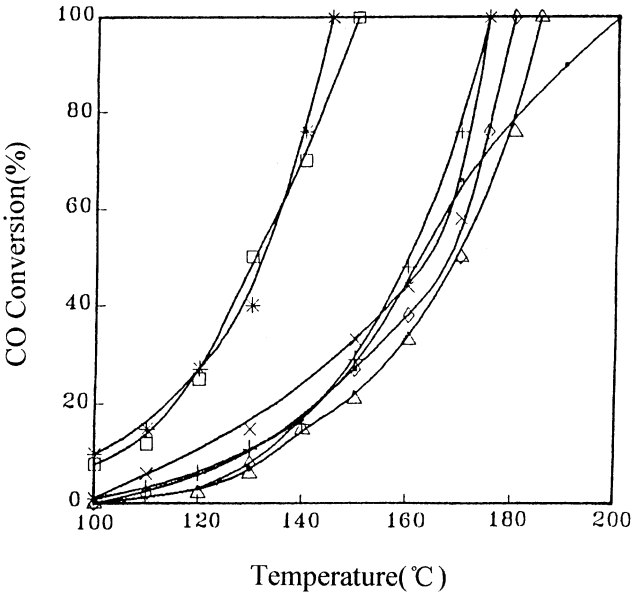

Figure 1. The CO oxidation activities of the samples (·) Co/γ-Al_2O_3, (×) Pt/γ-Al_2O_3, (◇) Pd/γ-Al_2O_3, (△) Rh/γ-Al_2O_3, (∗) Co–Pt/γ-Al_2O_3, (+) Co–Rh/γ-Al_2O_3, (□) Co–Pd/γ-Al_2O_3.

Co–Rh/γ-Al_2O_3 and Co/γ-Al_2O_3 have almost the same activity. The catalysts which have only noble metal composition also show good activity for CO oxidation. Comparing the activities of Co–Pt(Pd, Rh)/γ-Al_2O_3 with those of Pt(Pd, Rh)/γ-Al_2O_3, it is found that the temperatures for CO 100% conversion over Co–Pt(Pd, Rh)/γ-Al_2O_3 are 30–40°C lower than those of Pt(Pd, Rh)/γ-Al_2O_3. These results reveal that for CO oxidation there exists a pronounced catalytic synergy effect between cobalt and noble metals, especially between Co and Pt or Pd.

3.1.2. NO decomposition

The Co–Pt(Pd, Rh)/γ-Al_2O_3 catalysts possess high activities for NO decomposition during the initial period of reaction, however, with the increase of reaction time, the activities decrease obviously. Figure 2 shows the relationship between the reaction time and the NO conversion over Co–Pt(Pd, Rh)/γ-Al_2O_3 at the reaction temperature of 500°C. From figure 2, it is found that for NO decomposition, Co–Pt(Pd, Rh)/γ-Al_2O_3 catalysts exhibit high activities during the initial period, afterwards, the activities decrease markedly. When the reaction proceeds more than 1 h, the activities tend to remain unchanged. For Pt(Pd, Rh)/γ-Al_2O_3 catalysts, the NO decomposition activities are relatively low, and no obvious change is found with the reaction time increasing. The concentrations of the products N_2 and O_2 were also determined by the mass spectrometer. The relationship between the reaction time and the concentrations of N_2 and O_2 over Co–Pt/γ-Al_2O_3 catalyst is shown in figure 3. Comparing figure 2 with figure 3, it can be seen that the NO conversion and the N_2 production have the

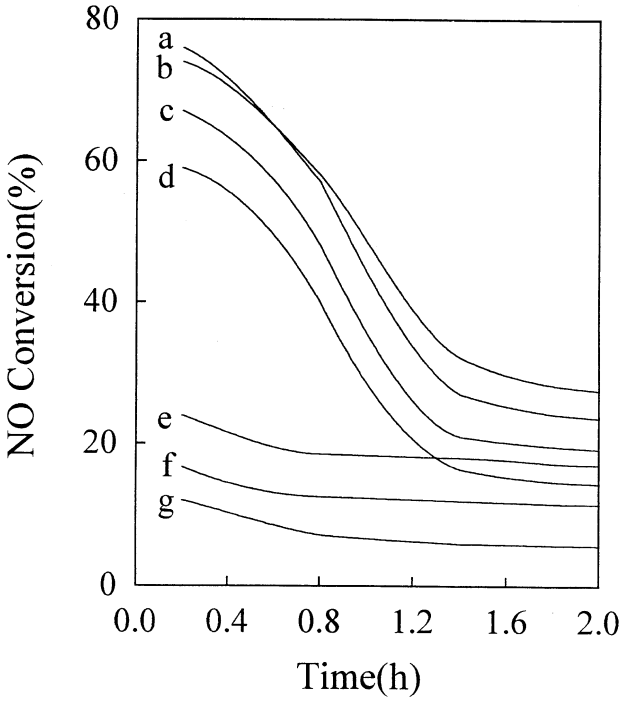

Figure 2. The relationship between NO conversion and reaction time over various catalysts. (a) Co–Pt/γ-Al_2O_3, (b) Co–Rh/γ-Al_2O_3, (c) Co–Pd/γ-Al_2O_3, (d) Co/γ-Al_2O_3, (e) Pt/γ-Al_2O_3, (f) Rh/γ-Al_2O_3, (g) Pd/γ-Al_2O_3.

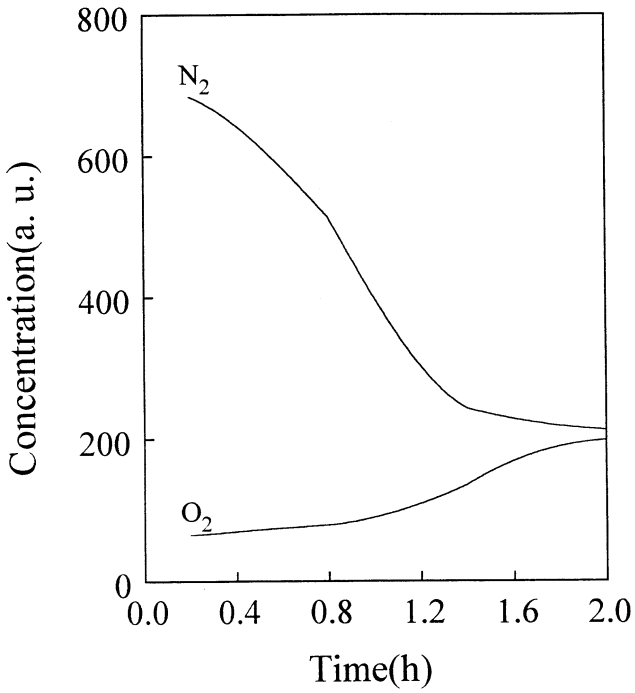

Figure 3. The concentrations of N_2 and O_2 during NO decomposition over Co–Pt/γ-Al_2O_3 catalyst.

same changing tendency, but the concentration of O_2 changes differently. If O_2 and N_2 are produced from NO decomposition, and desorb into gas phase completely, the concentrations of O_2 and N_2 must be equal to each other. In figure 3, the concentration of O_2 is much lower than that of N_2, especially during the initial period of the reaction. From this, it is inferred that there are at least some oxygen species which remain on the catalyst surface. At high reaction temperature, these oxygen species may react with the reduced cobalt phase on the catalyst surface. The obvious decrease of the activity may be resulted from the change of the active phases.

Comparing the activity of Co/γ-Al_2O_3 with those of Co–Pt(Pd, Rh)/γ-Al_2O_3, it is found that the presence of the small amount of noble metals has enhanced the activity of Co/γ-Al_2O_3 for NO decomposition to some extent, especially the platinum and rhodium.

3.1.3. NO selective reduction by C_2H_4

For NO selective reduction by C_2H_4, the samples calcined at 500°C and reduced by H_2 at 450°C are quickly oxidized by the excess oxygen in the reaction gas at high reaction temperature. The oxidized samples show the same black color as Co_3O_4. These samples show very low activities for NO selective reduction, the maximum conversion of NO is below 10%. In contrast, they show very high activities for C_2H_4 oxidation, the conversion of C_2H_4 reaches 100% at the reaction temperature of 450°C.

The samples calcined at 750°C exhibit a blue color (the typical color of $CoAl_2O_4$). After reduction by H_2 at 450°C, all the samples remain blue. This means that the $CoAl_2O_4$ phase has not been reduced. These samples possess relatively high activities for NO selective reduction. The activities of these samples are listed in table 1. The data in table 1 show that the conversions of NO and C_2H_4 are about 18 and 53% over Co/γ-Al_2O_3 at 450°C, respectively. With the addition of noble metals to Co/γ-Al_2O_3, both the conversions of NO and C_2H_4 are enhanced, the conversion of C_2H_4 increases more

Table 1
Activities of Co–Pt(Pd, Rh)/γ-Al_2O_3 catalysts for NO selective reduction by C_2H_4 at a reaction temperature of 450°C [a]

Sample	NO → N_2 conversion (%)	C_2H_4 → CO_2 conversion (%)
γ-Al_2O_3	6.0	18.0
Co/γ-Al_2O_3	18.2	53.0
Pt/γ-Al_2O_3	18.9	100
Pd/γ-Al_2O_3	14.7	100
Rh/γ-Al_2O_3	19.5	92.0
Co–Pt/γ-Al_2O_3	29.1	100
Co–Pd/γ-Al_2O_3	24.6	100
Co–Rh/γ-Al_2O_3	34.3	100

[a] Reaction conditions: NO = 1600 ppm, C_2H_4 = 1000 ppm, O_2 = 2.5%, $W/F = 0.6\,g\,s\,cm^{-3}$.

obviously. The rhodium exhibits the best promoting function.

3.2. Sample characterizations

3.2.1. XRD

The samples calcined at 500°C reduced by H_2 at 450°C were characterized by XRD. The XRD patterns of Co–Pt(Pd, Rh)/γ-Al_2O_3 are almost identical. So only the pattern of Co–Pt/γ-Al_2O_3 is shown in figure 4a. The pattern of Co/γ-Al_2O_3 is shown in figure 4b. Besides the peaks of γ-Al_2O_3, there are two very weak peaks at $2\theta = 44.4°$ and 51.5° in figure 4a; these two peaks correspond to metallic cobalt phase. The broad shape of the peaks and the invisibility of other diffracted peaks of Co^0 imply that the cobalt exists in highly dispersed state. In figure 4b, besides the peaks of the support, there are three peaks at the positions of $2\theta = 36.9°$, 65.3° and 31.2°. These peaks may come from Co_3O_4 or $CoAl_2O_4$, since Co_3O_4 and $CoAl_2O_4$ are indistinguishable by XRD. Considering that the samples are in reduced state and that Co_3O_4 is relatively easy to reduce [11,28,29], these peaks maybe correspond to $CoAl_2O_4$ or $CoAl_2O_4$-like spinel which is difficult to reduce [30,31]. Although no metallic cobalt is detected by XRD in Co/γ-Al_2O_3, the existence of Co^0 is possible because the amount of Co^0 may be below the detectable limit of XRD.

The samples used for NO decomposition were also investigated by the XRD method. The XRD patterns of Co–Pt(Pd, Rh)/γ-Al_2O_3 catalysts are similar to those in figure 4b. The two peaks of $2\theta = 44.4°$ and 51.5° disappear. The same color of the used Co–Pt(Pd, Rh)/γ-Al_2O_3 as Co_3O_4 indicates that the peaks at $2\theta = 36.9°$, 65.3° and 31.2° may be diffracted by Co_3O_4 phase. The oxidation of active phase is responsible for the decrease of NO decomposition activities.

The XRD patterns of Co–Pt(Pd, Rh)/γ-Al_2O_3 catalysts calcined at 750°C and reduced by H_2 at 450°C for NO selective reduction are also similar to those in figure 4b. The blue color of the samples indicates that the peaks in the position of $2\theta = 36.9°$, 65.3° and 31.2° come from the $CoAl_2O_4$ spinel. Combining the activity result with the XRD result, it is considered that $CoAl_2O_4$ is the main active phase for NO selective reduction, while Co_3O_4 is the main active phase for C_2H_4 oxidation.

3.2.2. XPS

The XPS spectrum of Co $2p_{3/2}$ for Co/γ-Al_2O_3 is shown in figure 5a. At the position of low binding energy, there are two peaks in figure 5a which appear at 778.3 and 780.9 eV, respectively. The binding energy of Co $2p_{3/2}$ for the first peak is very near to metallic cobalt [32], and that for the second peak it is near to $CoAl_2O_4$ [33,34]. At about 786.0 eV, there is also a broad weak peak. This is the typical satellite peak of Co^{2+}. The XPS spectra of Co $2p_{3/2}$ in Co–Pt(Pd, Rh)/γ-Al_2O_3 are similar to each other, so only the spectrum of Co $2p_{3/2}$ for Co–Pt/γ-Al_2O_3 is shown in figure 5b in which there is only one peak at about 778.3 eV, but no peaks appear at the position of high binding energy. These results prove that the cobalt on the surface of Co/γ-Al_2O_3 exists in the forms of Co^0 and $CoAl_2O_4$, while on the surface of Co–Pt(Pd, Rh)/γ-Al_2O_3 all cobalt exists as Co^0. The XPS results are in good agreement with that of XRD.

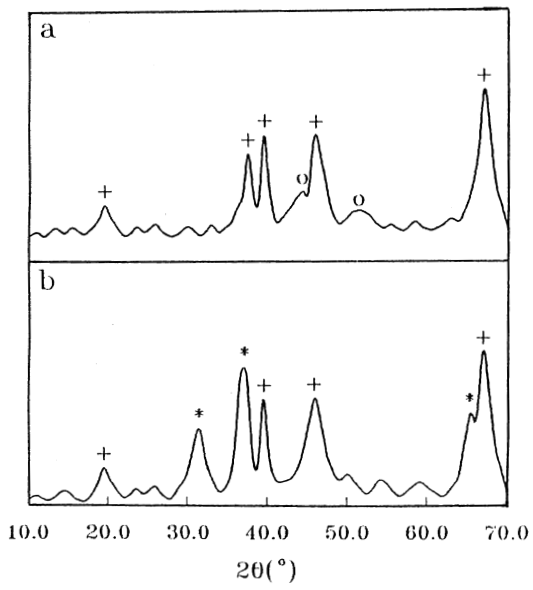

Figure 4. XRD spectra of Co–Pt/γ-Al_2O_3 and Co/γ-Al_2O_3. (a) Co–Pt/γ-Al_2O_3, (b) Co/γ-Al_2O_3; (+) γ-Al_2O_3 phase, (○) Co^0 phase, (∗) $CoAl_2O_4$ phase.

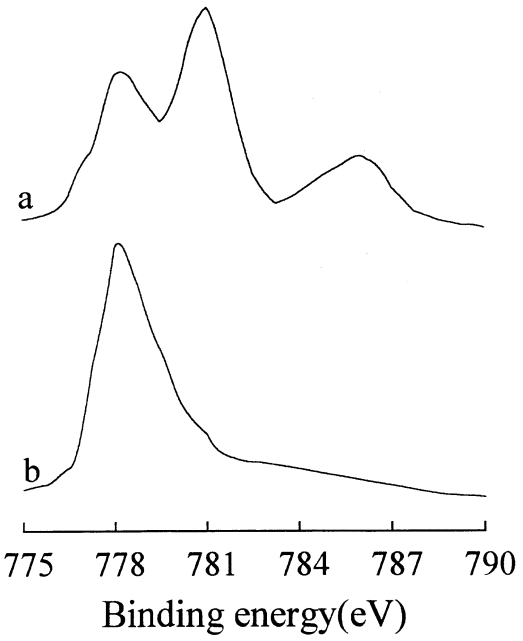

Figure 5. XPS spectra of Co $2p_{3/2}$ in Co/γ-Al_2O_3 and Co–Pt/γ-Al_2O_3. (a) Co/γ-Al_2O_3, (b) Co–Pt/γ-Al_2O_3.

3.2.3. XAFS

XANES of Co K-edge. The Co K-edge XANES spectra for the samples and model compounds are shown in figure 6. In the spectra of Co_3O_4 and $CoAl_2O_4$ (figures 6b and 6c), there is a weak absorption peak (1s→3d transition) at the pre-edge and a sharp absorption peak (1s→4p transition) above the absorption edge which is generally called white line. These features have been observed for many transition metal oxides. Comparing the spectrum of Co_3O_4 with that of $CoAl_2O_4$, it is found that both the absorption peaks of 1s→3d and 1s→4p of $CoAl_2O_4$ are stronger than those of Co_3O_4, and that the splitting of the white line of $CoAl_2O_4$ is more obvious than that of Co_3O_4. In addition, at the absorption edge, the spectrum of $CoAl_2O_4$ is seriously disturbed by a big shoulder, while the spectrum of Co_3O_4 is disturbed very slightly at the absorption edge. For Co metal, there is also a small shoulder at the absorption edge, but no 1s→3d peak at the pre-edge and no white line above the absorption edge. It has been indicated by some studies [35,36] that the pre-edge peak mainly results from the distorting tetrahedrally-coordinated Co^{2+} ions, and that the formation of a white line and its splitting are connected with the non-symmetry of coordination environment of central cobalt. The bulk Co metal has a highly symmetric coordination environment, therefore, no white line forms. In Co_3O_4, there are two kinds of cobalt ions, the distorting tetrahedrally-coordinated Co ions and the octahedrally-coordinated Co^{2+} ($Co^{2+}/Co^{3+} = 1/2$) ions. In $CoAl_2O_4$, all cobalt is in the form of distorting tetrahedrally-coordinated Co^{2+} ions, therefore, Co_3O_4 and $CoAl_2O_4$ have white lines, and the white line of $CoAl_2O_4$ splits more seriously than that of Co_3O_4.

Comparing the XANES spectra of the samples with those of the model compound, it is found that the spectrum of Co/γ-Al_2O_3 is similar to that of Co_3O_4 or $CoAl_2O_4$, and that the extent of the splitting of the white line is between those of Co_3O_4 and $CoAl_2O_4$. With the addition of noble metals to Co/γ-Al_2O_3, the splitting of the white line becomes less serious. On the basis of XRD and XPS results and the above analysis, the formation of 1s→3d and 1s→4p peaks and the splitting of the white line for Co/γ-Al_2O_3 may be resulted from the Co^{2+} ions in $CoAl_2O_4$-like spinel. Although the cobalt in Co–Pt(Pd, Rh)/γ-Al_2O_3 is in metallic state according to XRD and XPS results, it has a different coordination environment from the Co metal used as a model compound because the cobalt in Co–Pt(Pd, Rh)/γ-Al_2O_3 is dispersed on the surface of γ-Al_2O_3 and generally has much smaller particle size. Therefore, the cobalt in Co–Pt(Pd, Rh)/γ-Al_2O_3 has less symmetric coordination environment than the Co metal used as model compound.

EXAFS of Co K-edge. Six absorption curves of Co K-edge of the samples and model compounds were recorded. The EXAFS functions were first Fourier-transformed from k space to r space to obtain the radial structure functions (RSFs). The RSFs of model compounds and the samples are shown in figures 7 and 8, respectively. For Co–Pt(Pd, Rh)/γ-Al_2O_3, the RSFs are similar to that of Co metal. There is only one coordination shell appearing at 0.212 nm. Considering the scattering phase shift, this coordination shell corresponds to the Co–Co shell in Co metal at the position of 0.250 nm. In the RSF of Co/γ-Al_2O_3, there are two coordination shells appearing at 0.147 and 0.266 nm, respectively. The

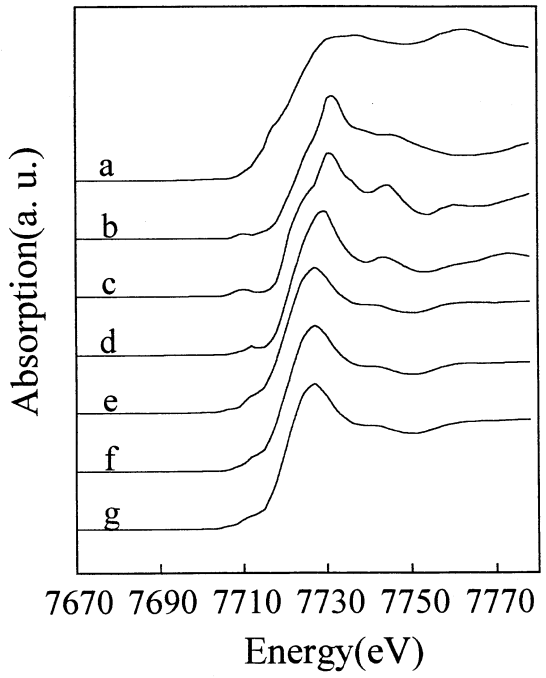

Figure 6. XANES spectra of Co K-edge of the samples and model compounds. (a) Co metal, (b) Co_3O_4, (c) $CoAl_2O_4$, (d) Co/γ-Al_2O_3, (e) Co–Pt/γ-Al_2O_3, (f) Co–Pd/γ-Al_2O_3, (g) Co–Rh/γ-Al_2O_3.

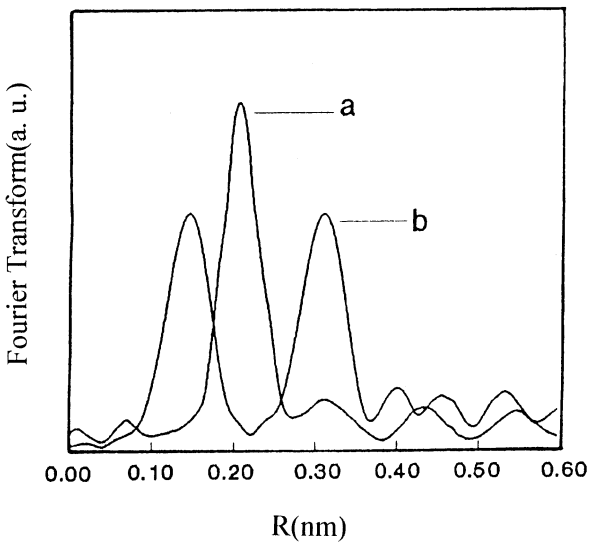

Figure 7. The radial structure functions of Co K-edge of model compounds. (a) Co metal, (b) $CoAl_2O_4$.

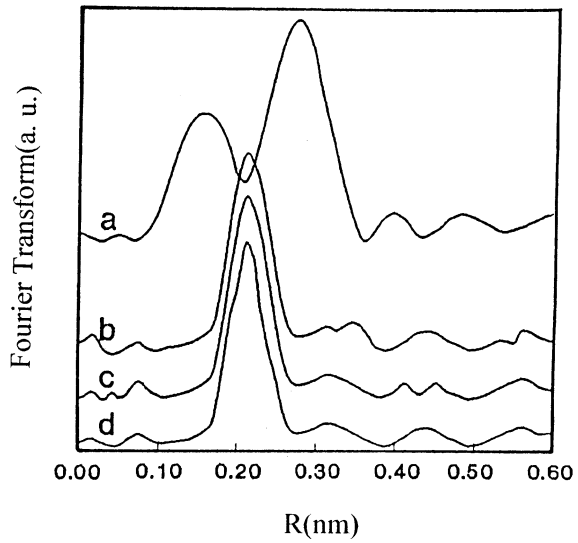

Figure 8. The radial structure functions of Co K-edge of the samples. (a) Co/γ-Al_2O_3, (b) Co–Pt/γ-Al_2O_3, (c) Co–Pd/γ-Al_2O_3, (d) Co–Rh/γ-Al_2O_3.

first shell can be fitted by the Co–O shell in $CoAl_2O_4$ (0.143 nm), but the second shell appearing at 0.266 nm cannot be fitted by either the Co–Co shell in Co metal (0.212 nm) or the Co–Co shell in $CoAl_2O_4$ (0.312 nm) because of the big difference in interatomic distance. According to the results of XRD and XPS, the second shell in Co/γ-Al_2O_3 may be contributed to both Co^0 and $CoAl_2O_4$.

The structural parameters of the first shells of the model compounds and catalyst samples are shown in table 2. From the interatomic distance (R) of the Co–Co shell in table 2, it is inferred that the cobalt in Co–Pt(Pd, Rh)/γ-Al_2O_3 exists in the form of metallic state, and that the cobalt in Co/γ-Al_2O_3 may exist as the mixture of Co^0 and $CoAl_2O_4$-like spinel. Compared with Co metal, the cobalt in Co–Pt(Pd, Rh)/γ-Al_2O_3 has much smaller coordination number (N). This shows that the cobalt in the samples has high dispersion, especially in the samples containing Pt or Pd.

Table 2
Best-fitting values of structural parameters of the first coordination shell for the samples containing cobalt from EXAFS data

Sample	First coordination shell		
	shell	N	R(nm)
Co–Pt/γ-Al_2O_3	Co–Co	4.5	0.251
Co–Pd/γ-Al_2O_3	Co–Co	5.3	0.251
Co–Rh/γ-Al_2O_3	Co–Co	6.0	0.251
Co/γ-Al_2O_3	Co–O	2.8	0.200
$CoAl_2O_4$ [a]	Co–O	4.0	0.195
Co metal [a]	Co–Co	12.0	0.250

[a] The structural parameters come from ref. [37].

3.2.4. TPR

The results of XRD, XPS and XAFS have shown that the reduced Co–Pt(Pd, Rh)/γ-Al_2O_3 and Co/γ-Al_2O_3 have different cobalt phases. The enhancement for cobalt phase reduction by noble metals may be related to hydrogen spillover. The hydrogen species spilled from noble metals to cobalt phase decrease the activation energy of dissociated adsorption of hydrogen over the cobalt phase, and make the cobalt phase reduced more easily.

To investigate the possibility of hydrogen spillover effect, the reduced samples were oxidized at 500°C in air for 1 h, then they were used for TPR measurement. Figure 9 shows the TPR profiles of the oxidized samples. There are two reduction peaks for Co/γ-Al_2O_3. No reduction peaks are detected for Pt(Pd, Rh)/γ-Al_2O_3 below 700°C. This means that the TPR peaks in figure 9 come from the reduction of cobalt phase. With the addition of noble metals to Co/γ-Al_2O_3, both peaks shift to lower temperatures. The temperatures of the first peaks decrease by about 99–122°C, and those of the second peaks decrease by about 92–134°C, and the relative peak area (see table 3) increases a little. Similar results for cobalt-based catalysts are obtained by other studies [17–20]. The decrease of TPR peak temperature has been thought to be connected to the spillover of hydrogen species from noble metals to cobalt phases, and the increase of peak area is assigned to the enhanced dispersion of cobalt phase by noble metals. For Co/γ-Al_2O_3 there are two reduction peaks appearing at 448 and 690°C, respectively. For pure Co_3O_4, there is only one reduction peak at 378°C. It has been reported [11,28–31] that Co_3O_4 is relatively easy to reduce (below 450°C), while $CoAl_2O_4$ is very difficult to reduce (above 700°C). Therefore, the first peak may correspond to the reduction of highly dispersed Co_3O_4, the second may correspond to a $CoAl_2O_4$-like phase. The results of XAFS have shown that when the Co/γ-Al_2O_3 sample is calcined at 500°C, some cobalt phase react with γ-Al_2O_3 to form a

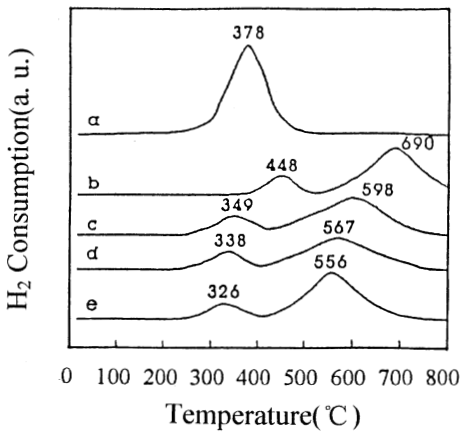

Figure 9. The TPR profiles of the samples. (a) Co_3O_4, (b) Co/γ-Al_2O_3, (c) Co–Rh/γ-Al_2O_3, (d) Co–Pd/γ-Al_2O_3, (e) Co–Pt/γ-Al_2O_3.

Table 3
The relative area of TPR, TPO-MS and TPD peaks for Co–Pt(Pd, Rh)/γ-Al_2O_3 samples

Sample	Relative area [a]		
	TPR peaks	TPO-MS peaks	TPD peaks
Co/γ-Al_2O_3	1.0(448), 3.5(690)	4.5(320)	1.0(166), 2.7(492)
Co–Pt/γ-Al_2O_3	1.2(326), 3.8(556)	6.4(260)	1.7(181), 5.2(509)
Co–Pd/γ-Al_2O_3	1.2(338), 3.7(567)	6.2(260)	1.6(170), 4.9(498)
Co–Rh/γ-Al_2O_3	1.1(349), 3.9(598)	5.6(300)	1.6(153), 4.6(502)

[a] The peak top temperature is listed in parentheses.

$CoAl_2O_4$-like spinel. The distance of the first coordination shell (Co–O) is a little longer than that of the model compound $CoAl_2O_4$, therefore, the reduction peak temperature is lower than that of $CoAl_2O_4$.

The TPR results have indicated that the presence of noble metals has enhanced the reduction of cobalt phases. The difference in cobalt phase between the reduced Co–Pt(Pd, Rh)/γ-Al_2O_3 and Co/γ-Al_2O_3 may be caused by hydrogen spillover during the preparation.

3.2.5. TPD

The O_2-TPD profiles of the samples are given in figure 10. Two kinds of oxygen species desorb from Co–Pt(Pd, Rh)/γ-Al_2O_3 catalysts. The first kind of oxygen species desorb at low temperature (below 200°C), while the second desorb at relatively high temperature (around 500°C). Generally, the adsorbed oxygen changes by the following procedures:

$$O_2(ad) \rightarrow O_2^-(ad) \rightarrow O^-(ad) \rightarrow O^{2-}(lattice)$$

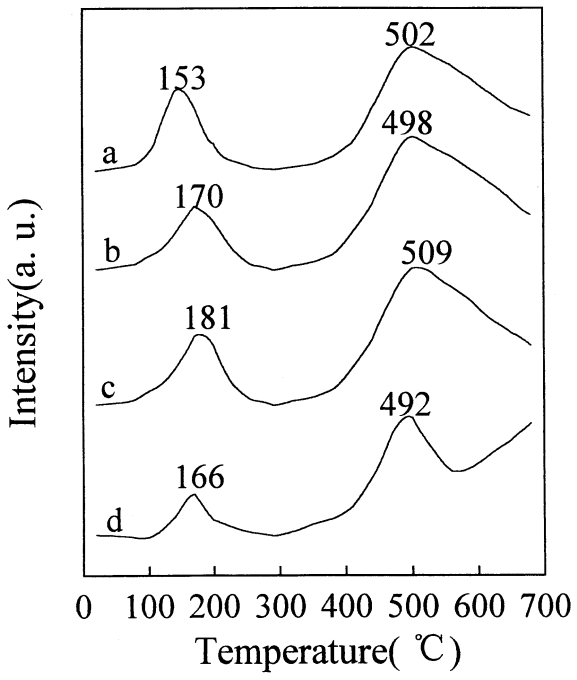

Figure 10. The O_2-TPD profiles of the samples. (a) Co–Rh/γ-Al_2O_3, (b) Co–Pt/γ-Al_2O_3, (c) Co–Pd/γ-Al_2O_3, (d) Co/γ-Al_2O_3.

The physically adsorbed oxygen and O_2^-(ad) species are relatively easy to desorb, while the lattice O^{2-} species are very difficult to desorb. In figure 10, the low temperature of the first peak implies that the desorbed oxygen species may be physically adsorbed oxygen or O_2^-(ad) species. Generally, the lattice oxygen species desorb very slowly. The peak shape is not symmetric. In figure 10, the second peak has good symmetry, and the temperature is not very high, therefore, it is more reasonable to assign this peak to the desorption of O^- species. For Co/γ-Al_2O_3 catalyst (figure 10d), besides the two peaks, there is another one at very high temperature (> 700°C). The results of XRD, XPS and EXAFS have proved that there is a $CoAl_2O_4$-like phase in Co/γ-Al_2O_3 which is very stable. The third peak perhaps comes from the lattice oxygen in the $CoAl_2O_4$-like phase.

From the relative peak area (see table 3), it is found that, with the addition of noble metals to Co/γ-Al_2O_3, the areas of the first two peaks increase obviously. This may result from the oxygen spillover from noble metals to cobalt phases.

3.2.6. TPO

The oxygen-consumption curves for various catalysts recorded by a quadrupole mass spectrometer are shown in figure 11. For Pt(Pd, Rh)/γ-Al_2O_3, no obvious oxygen-consumption peaks are found because of the very low contents of noble metals in the catalysts. For Co/γ-Al_2O_3, an obvious oxygen-consumption peak appearing at 320°C is detected. When noble metals are added to Co/γ-Al_2O_3, not only does the position shift to lower temperatures, but also the peak area increases obviously (see table 3). The smaller area of Co/γ-Al_2O_3 than Co–Pt(Pd, Rh)/γ-Al_2O_3 is due to the presence of $CoAl_2O_4$-like spinel in Co/γ-Al_2O_3 which was formed during the calcination in air. Comparing the areas of Co–Pt(Pd, Rh)/γ-Al_2O_3, it is found that the order of the areas is consistent with the cobalt dispersion from the coordination number of the Co–Co shell (see table 2). As to the decrease of the oxygen-consumption peak temperature for Co–Pt(Pd, Rh)/γ-Al_2O_3, the oxygen spillover from noble metals to cobalt phase may be the most reasonable explanation.

Combined with the results of O_2-TPD, the spilled-over oxygen is thought to be one of the main contributors to the enhancement of the catalytic activities of Co–

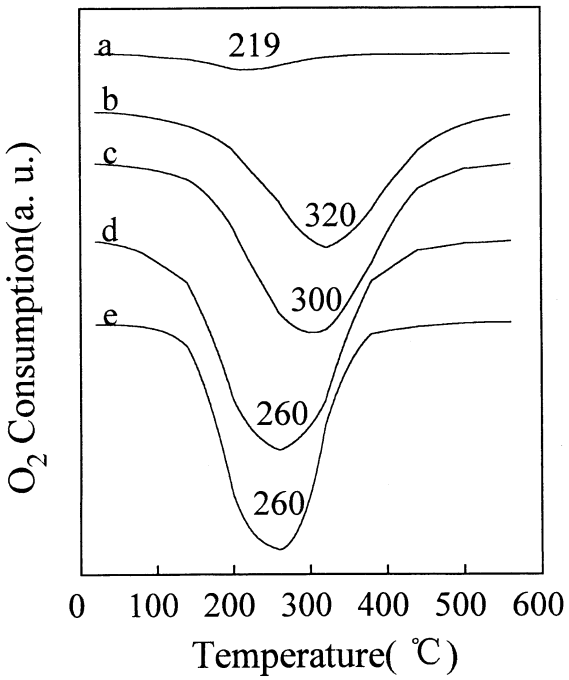

Figure 11. The oxygen-consumption curves during TPO measurement. (a) Pt/γ-Al_2O_3, (b) Co/γ-Al_2O_3, (c) Co–Rh/γ-Al_2O_3, (d) Co–Pt/γ-Al_2O_3, (e) Co–Pd/γ-Al_2O_3.

Pt(Pd, Rh)/γ-Al_2O_3. For CO oxidation, it is easy to understand that the spilled-over oxygen species are very active which helps to activate and oxidize CO molecules.

4. Conclusions

(1) The γ-Al_2O_3-supported cobalt catalysts promoted with a small amount of noble metals are good catalysts for CO oxidation; the noble metals enhance the activities for CO oxidation and for C_2H_4 oxidation during NO selective reduction by C_2H_4, especially platinum and palladium. The main active cobalt phase for CO oxidation is Co^0.

(2) For NO decomposition, the reduced samples show very high activities during the initial period of the reaction. But the oxygen produced from NO decomposition oxidizes the surface cobalt phase and causes the sharp decrease of catalytic activities. The activity of Co_3O_4 phase is much lower than that of Co^0.

(3) For NO selective reduction by C_2H_4, the surface Co^0 is oxidized into Co_3O_4 by the excess oxygen in the reaction gas very quickly. The Co_3O_4 phase exhibits very low activity for NO selective reduction by C_2H_4, while all the samples with blue color exhibit better activities. $CoAl_2O_4$ is thought to be the main SCR active sites, and Co_3O_4 is the main active sites for C_2H_4 complete oxidation.

(4) The results of XRD, XPS and XAFS indicate that all the cobalt in Co–Pt(Pd, Rh)/γ-Al_2O_3 catalysts which were calcined at 500°C and reduced at 450°C exists as Co^0, while in Co/γ-Al_2O_3 only part of the cobalt has been reduced to zero valence, the rest exists as $CoAl_2O_4$-like spinel. The difference of the active phases between Co–Pt(Pd, Rh)/γ-Al_2O_3 and Co/γ-Al_2O_3 is one of the main reasons for their activity difference. The coordination number of Co–Co shell from EXAFS shows that the cobalt is highly dispersed in Co–Pt(Pd, Rh)/γ-Al_2O_3 catalysts.

(5) The prominent decrease of TPR peak temperatures of Co–Pt(Pd, Rh)/γ-Al_2O_3 has shown that the presence of noble metals enhances the reduction of cobalt phases. The difference of cobalt phases between Co/γ-Al_2O_3 and Co–Pt(Pd, Rh)/γ-Al_2O_3 may be caused by hydrogen spillover for the latter during the reduction.

(6) From the results of O_2-TPD and TPO-MS, it is inferred that the noble metals enhance the adsorption of oxygen on Co–Pt(Pd, Rh)/γ-Al_2O_3 catalysts and the oxidation of Co^0. The decrease of TPO peak temperature implies that the oxygen species spill over from noble metals to cobalt phase. During the CO oxidation, the spillover of oxygen may be one of the main contributors of noble metals to activity enhancement.

Acknowledgement

The project is supported by "Ford-China Research and Development Fund No. 9712301" and "National Natural Science Foundation of China No. 29573122". The supply of programs for EXAFS calculation from Professor Kun-Quan Lu and the support from BSRF NL are gratefully acknowledged.

References

[1] T.J. Lawton and R.J. Gower, Plat. Met. Rev. 38 (1994) 160.
[2] J.T. Kummer, J. Phys. Chem. 90 (1986) 4747.
[3] J.R. Gonzalez-Velasco, J. Entrena, J.A. Gonzalez-Marcos, J.I. Gutierre et al., Appl. Catal. B 3 (1994) 191.
[4] T.J. Truex, R.A. Searles and D.C. Sun, Plat. Met. Rev. 36 (1992) 2.
[5] Y. Li, T.L. Slager and J.N. Armor, J. Catal. 150 (1994) 388.
[6] Y. Li and J.N. Armor, Appl. Catal. B 2 (1993) 239.
[7] X. Zhang, A.B. Walters and M.A. Vannice, J. Catal. 155 (1995) 290.
[8] X. Zhang, A.B. Walters and M.A. Vannice, J. Catal. 146 (1994) 568.
[9] X. Zhang, A.B. Walters and M.A. Vannice, Appl.Catal. B 4 (1994) 237.
[10] E. Iglesia, S.L. Soled and R.A. Fiato, J. Catal. 137 (1992) 212.
[11] M. Meng, P.Y. Lin and S.M. Yu, Chinese J. Chem. Phys. 8 (1995) 66.
[12] R.J. Voorhoeve, D.W. Johnson, J. Remeika and P.K. Gallagher, Sci. 195 (1977) 827.
[13] J.M. Tascon, L.G. Tejuca and C.H. Rochester, J. Catal. 95 (1985) 558.

[14] H. Hamada, Y. Kintaichi, M. Sasaki and T. Ito, Appl. Catal. 75 (1991) L1.
[15] M. Shelef, K. Otto and H. Gandh, Atmos. Environ. 3 (1969) 107.
[16] Y. Teraoka, H. Fukuda and S. Kagawa, Chem. Lett. (1990) 1, 1069.
[17] P.Y. Lin, M. Skoglundh, L. Lowendahl, J.E. Otterstedt et al., Appl. Catal. B 6 (1995) 237.
[18] D. Schanke, S. Vada, E.A. Blekkan, A.M. Hilmen, A. Hoff and A. Holmen, J. Catal. 156 (1995) 85.
[19] L. Guczi, T. Hoffer, Z. Zsoldos, S. Zyade, G. Maire and F. Garin, J. Phys. Chem. 95 (1991) 802.
[20] V.M. Belousov, J. Stoch, I.V. Batcherikova, E.V. Rozhkova and L.V. Lyashenko, Appl. Surf. Sci. 35 (1988) 481.
[21] A.S. Sass, V.A. Shvet, G.A. Saveleva and V.B. Kazanskii, Kinet. Katal. 26 (1985) 1149.
[22] H.F.J. van't Blik and R. Prins, J. Catal. 97 (1986) 188.
[23] Z. Zsoldos, T. Hoffer and L. Guczi, J. Phys. Chem. 95 (1991) 795.
[24] Z. Zsoldos and L. Guczi, J. Phys. Chem. 96 (1992) 9393.
[25] S. Zyade, F. Garin and G. Maire, New J. Chem. 11 (1987) 429.
[26] U. Bardi, B.C. Beard and P.N. Ross, J. Catal. 124 (1990) 22.
[27] U. Bardi, A. Atrei, G. Rovida and M. Torrini, Surf. Sci. Lett. 282 (1993) L365.
[28] P. Arnoldy and J.A. Moulijn, J. Catal. 93 (1985) 38.
[29] W.J. Wang and Y.W. Chen, Appl. Catal. 7 (1991) 223.
[30] K.S. Chung and F.E. Massoth, J. Catal. 64 (1980) 320.
[31] M. Meng, P.Y. Lin and S.M. Yu, Chinese J. Chem. Phys. 8 (1995) 176.
[32] C.D. Wagner, W.M. Riggs, L.E. Davis, J.F. Moulder and G.E. Muilenberg, *Handbook of X-ray Photoelectron Spetroscopy* (Perkin-Elmer Corp. Physical Electronics Division, USA, 1979).
[33] Y. Okamoto, T. Imanaka and S. Teranishi, J. Catal. 65 (1980) 448.
[34] Y. Okamoto, T. Adachi, K. Nagata, M. Odawara and T. Imanaka, Appl. Catal. 73 (1991) 249.
[35] R.B. Greegor, F.W. Lytle, R.L. Chin and D.M. Hercules, J. Phys. Chem. 85 (1981) 1232.
[36] H.W. Xiang, T.D. Hu, B. Zhong, S.Y. Peng, Y.N. Xie, D.X. Huang and X.N. Chen, Chinese J. Chem. Phys. 8 (1995) 75.
[37] G. Sankar, S. Vasudevan and C.N.R. Rao, J. Phys. Chem. 91 (1987) 2011.